6. Influenza virus PR8 and CpG 1826 oligonucleotide induce differential activation of plasmacytoid dendritic cells

6.1. Introduction

pDCs exhibit potent functions in infectious, autoimmune disease and cancer in both humans and mice [43, 44, 171]. As important sentinels for pathogen-associated molecular patterns (PAMPs), in particular viruses, pDCs are the prime producers of IFN-α and are therefore also called natural type I interferon-producing cell (IPC) [38, 42, 96]. In a model of respiratory syncytial virus (RSV) infection, depletion of pDCs resulted in decreased viral clearance and increased pulmonary pathology [172, 173]. PDC depletion also led to impaired induction of cytotoxic T cells during herpes simplex virus (HSV) infection [174]. Besides their production of IFN-α, activated pDCs are able to release a variable panel of cytokines and chemokines. These mediators can cross-talk to other cells of the adaptive immune system thereby contributing to the differentiation of B cells, augmenting the activity of NK cells, and attracting T and NK cells during viral infections [92, 96, 97, 120, 123, 175]. In contrast to their immune-response promoting effects in antiviral immunity, there is increasing evidence that pDCs may contribute to the maintenance of tolerance by preventing asthmatic reactions and inducing regulatory T cells [113-115, 161]. Moreover, pDCs have been implicated in the production of immunosuppressive mediators such as indoleamine 2,3-dioxygenase (IDO) with negative effects in anti-tumor and anti-HIV responses [118, 119]. Given this wide array of effects, activated pDCs may adopt functionally distinct differentiation states. However, while it has been speculated that such states exist [176], there is little data on how these differentiation states are induced and/or regulated.

The response of pDCs to pathogens and their components has been explored by the use of model ligands for two main TLRs, TLR7 and TLR9, that are expressed by pDCs [58, 59]. Ligands for TLR7 include synthetic compounds of the family of imidazoquinolines [67] and viral ss-RNA, which have been shown to activate pDCs [63, 64]. TLR9 on pDCs can be

triggered by specific unmethylated CpG-containing motifs common to both bacterial and viral DNA with a core sequence (GACGTT) that is highly stimulatory for TLR9 [68]. The traditional readout for evaluating the effects of such stimuli on pDCs has been the production of type I interferons and a few select cytokines, such as interleukin IL-12. This has led to the discovery that specific compounds induce different amounts of IFNs in pDC. For example, CpG-A ODN are potent inducers of IFN-α, whereas CpG-B ODN elicit a weak IFN-α release [68, 177]. In addition, the induction of T cell proliferation and differentiation is also commonly used to examine the effects of certain stimuli on pDCs. However, a full phenotypic and functional profile of specialized pDC populations remains elusive.

The work presented in this chapter is the first study to define two phenotypically and functionally distinct states of pDCs following their activation with influenza virus A/PR/8 and CpG 1826 ODN, two prototypic ligands for TLR7 and TLR9, respectively. We could induce differentiation of pDCs into either major type I producing cells or pDCs with higher expression of costimulatory molecules and high production of pro-inflammatory cytokines. The results of the characterization of these distinct pDC populations performed in this study may be useful in the future to selectively target their functions for the treatment of microbial and inflammatory diseases.

6.2. Results

6.2.1. Transgenic DPE^{GFP} mice harbor pDCs that express high levels of GFP

For the data shown here, we used a previously developed transgenic mouse strain, termed DPE^{GFP}, in which the enhanced green fluorescent protein (EGFP) is expressed under the control of the minimal CD4 promoter and the distal and proximal enhancer of the murine CD4 locus [178, 179] (Figure 8).

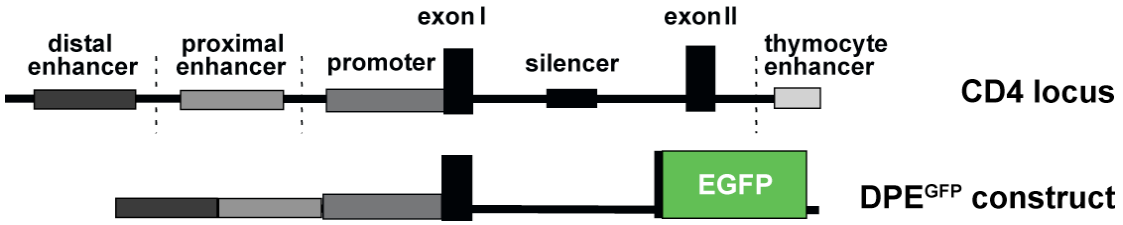

Figure 8: Schematic of regulatory elements in the murine CD4 locus and the DNA construct for the transgenic mouse strain DPE^{GFP}.

The green fluorescent protein (GFP) is driven by a distal and a proximal enhancer element (DPE) upstream of the minimal promoter sequence of the murine CD4 locus.

The construct lacks an intronic silencer element that suppresses CD4 expression in mature CD8$^+$ T cells [163, 165, 180]. Thus, GFP is expressed in all naïve T cells (see also Figure 9). A single cell suspension prepared from the spleen of a DPE^{GFP} mouse was stained for CD3, a marker for T cells, and CD19, a marker for B cells, and GFP transgene expression in those subsets was examined by flow cytometry. Whereas most of the CD19$^+$ B cells were GFP$^-$, the majority of CD3$^+$ T cells expressed GFP. In addition to T cells, another subset of cells was discovered to express the transgene GFP at high levels (GFP^{hi}). After further

analysis, this subset of cells was found to express intermediate level of CD11c, a dendritic cell marker. However, conventional CD11c^{hi} cells in DPE^{GFP} mice were GFP^{-}.

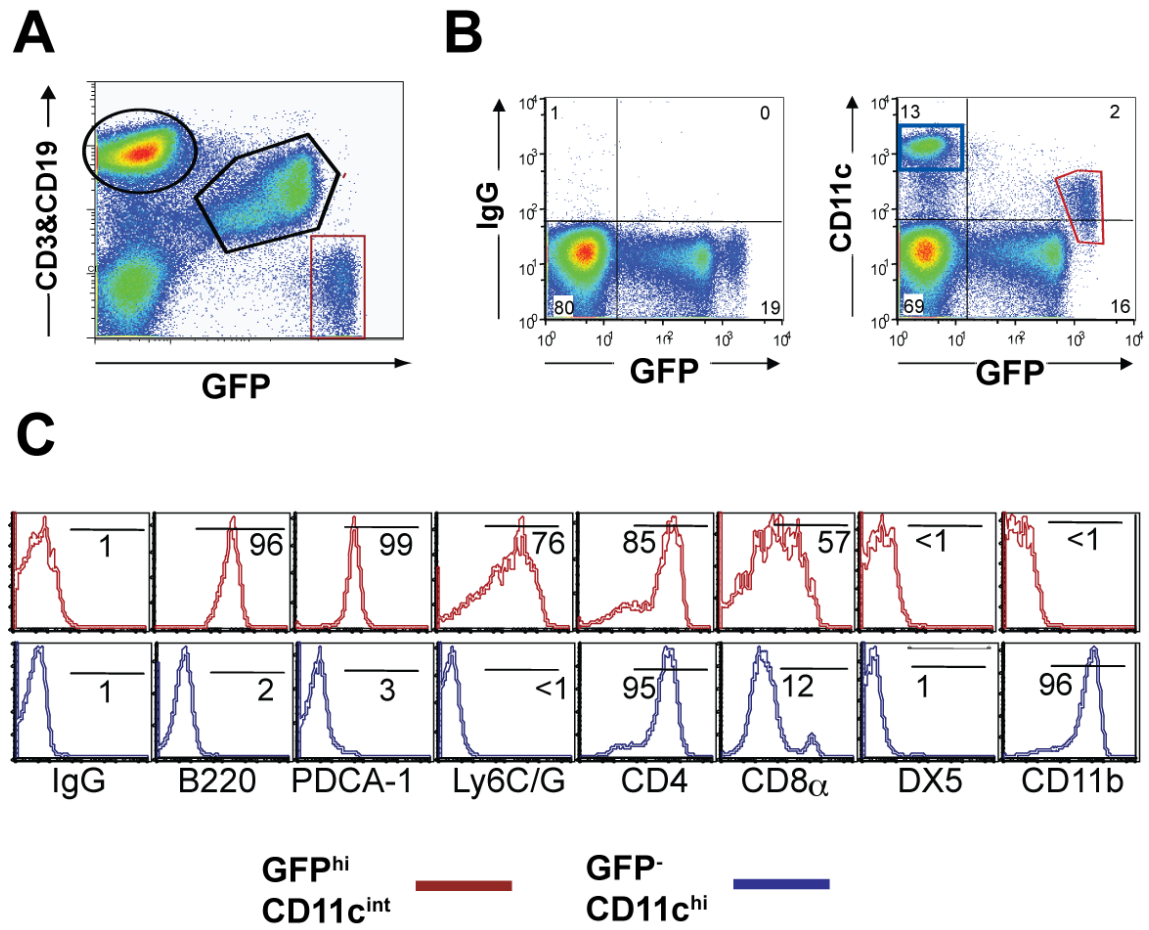

Figure 9: GFP^{hi} cells in the DPE^{GFP} mouse express intermediate levels of CD11c.

(**A**) Representative flow cytometry profile of gradient-enriched splenocytes from a DPE^{GFP} mouse, which were stained with αCD19 and αCD3 to identify B cells and T cells. Cell populations represent: GFP^{-} CD19^{+} B cells (black oval), GFP^{+} CD3^{+} T cells (black polygon) and a non-lymphocyte population that expresses high levels of GFP (red gate). (**B**) Splenocytes as in (**A**) were stained with a control antibody (left plot) or αCD11c (right plot). Cells with high expression levels of GFP (GFP^{hi}) express intermediate levels of CD11c compared to CD11c^{hi} cells, which are GFP negative. Numbers depict percentage of cells in each quadrant. (**C**) Gates were set on GFP^{-} CD11c^{hi} cells (red) and GFP^{hi} CD11c^{int} cells (blue) (see **B**, right plot) and expression of lineage markers was analyzed. Numbers represent frequency of marker positive cells.

Phenotypic characterization of GFP^{hi} CD11c^{int} CD3^{-} CD19^{-} cells revealed that they expressed none of the following lineage markers: NK1.1 and DX5 (NK cells and NKT cells), CD11b (myeloid cells), and F4/80 (macrophages). However, GFP^{hi} cells exhibited all the phenotypic characteristics ascribed to murine plasmacytoid dendritic cells, i.e. they expressed B220, PDCA-1 and Ly6C/G (Figure 9C).

Next, it was assessed whether all pDCs in DPE^{GFP} mice expressed GFP. Splenocytes from DPE^{GFP} mice were stained for B220, CD11c, and Ly6C/G, and gates were set on the B220^{+} CD11c^{int} population (Figure 10). Within this gate, two distinct cell populations could be distinguished: one subset was GFP^{-} Ly6C/G^{-} and presumably represents mDC precursors. The other subset expressed high levels of GFP and Ly6C/G, and also co-expressed PDCA-1 (not shown). The fact that all CD11c^{int} B220^{+} Ly6C/G^{+} PDCA-1^{+} cells co-expressed GFP indicates that all pDCs in DPE^{GFP} mice are GFP^{+}.

Collectively, these results indicate that GFP^{hi} cells in DPE^{GFP} mice fulfill the phenotypic criteria of pDCs.

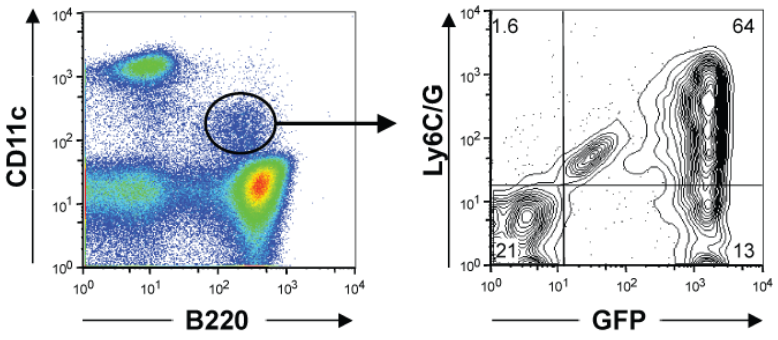

Figure 10: All pDCs in DPE^{GFP} mice express GFP at high levels.

B220^{+} CD11c^{int} pDCs (left plot, gate) were analyzed for co-expression of GFP and Ly6C/G. Cells in the gate were mostly Ly6C/G^{+} and co-expressed GFP.

6.2.2. GFP^{hi} pDCs respond to Flt-3 ligand and can be expanded as the only cell subset that expresses GFP in DPE^{GFP}xRAG-1$^{-/-}$ mice

Next, the ability of GFP^{hi} pDCs to respond to Flt-3 ligand (Flt-3L) was tested. DPE^{GFP} mice were implanted subcutaneously with B16F10 tumor cells modified to express recombinant Flt-3L [168]. 12-14 days later, the number of pDCs in various organs was determined. As shown in Figure 11A, Flt-3L treatment resulted in a marked increase in the numbers of circulating GFP^{hi} cells in peripheral blood as well as secondary organs such as the spleen, peripheral LN (PLN), mesenteric LN (MLN) and Peyer's patches (PP). Whereas the percentage of pDCs in bone marrow (BM) remained unchanged, pDCs also increased significantly in lung and liver compared to wild-type mice.

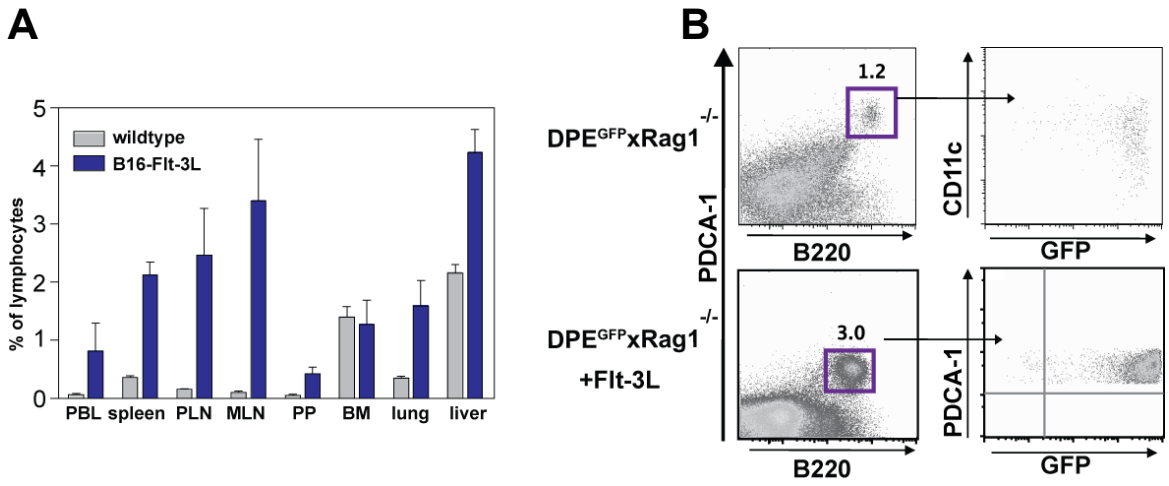

Figure 11: pDC expansion in response to Flt-3 ligand.

(**A**) DPE^{GFP} mice were implanted subcutaneously with B16-Flt-3L cells. 12-14 days later, organs were harvested and analyzed for the presence of B220^{+} CD11c^{int} GFP^{hi} cells. (**B**) Splenocytes of a DPE^{GFP}xRAG-1$^{-/-}$ mouse with (bottom) or without (top) implanted B16F10-Flt-3 ligand (Flt-3L)-expressing tumor cells were stained for B220 and mPDCA-1 and analyzed for co-expression of CD11c and GFP.

Despite the fact that pDCs express higher levels of GFP than T cells in DPE^{GFP} mice, their unequivocal identification *in vivo* is confounded by the much higher abundance of T cells. To circumvent this, DPE^{GFP} mice were crossed with RAG-1-deficient animals that lack B and T lymphocytes (DPE^{GFP}xRAG-1$^{-/-}$ mice). B16-Flt-3L-tumor implantation in DPE^{GFP}xRAG-1$^{-/-}$ mice led to a marked increase of the percentage as well as of total numbers of GFP^{hi} B220^{+} PDCA-1^{+} pDCs (Figure 11B and data not shown). Similar to splenocytes of DPE^{GFP} mice, all B220^{+} mPDCA-1^{+} cells were GFP^{hi} and expressed intermediate levels of CD11c, indicating that all pDCs in DPE^{GFP}xRAG-1$^{-/-}$ mice with or without Flt-3L-treatment express GFP (Figure 11B). Extensive phenotypic analysis of pDCs isolated from untreated, Flt-3L-treated mice and DPE^{GFP} mice showed no differences in the expression levels of costimulatory molecules and adhesion molecules [41] (see chapter 2 and data not shown), indicating that pDCs developed normally in the absence of T and B lymphocytes.

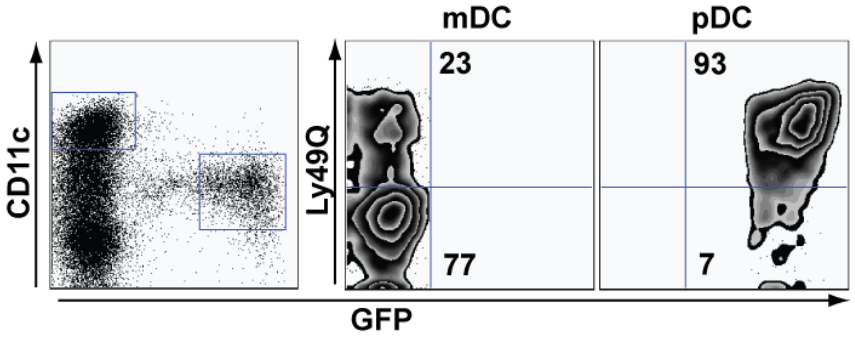

Figure 12: The majority of pDCs from Flt-3L-treated mice are Ly49Q^{+}.

Splenocytes of a Flt-3L-treated DPE^{GFP}xRAG-1$^{-/-}$ mouse were stained for CD11c and Ly49Q expression and analyzed by flow cytometry. Live cells were gated on GFP^{-} CD11c^{hi} cells (mDCs) and on GFP^{+} CD11c^{int} (pDCs). Numbers represent percentages of Ly49Q positive and negative cells within the gated population.

Recently, a pDC precursor has been described in the bone marrow of mice that is negative for Ly49Q, an inhibitory receptor, while more mature pDCs express Ly49Q [55, 56]. In order to determine whether this precursor could be identified in peripheral organs after B16-Flt-3L implantation, splenocytes of Flt-3L-treated DPE^{GFP}xRAG-1$^{-/-}$ mice were stained for Ly49Q and analyzed by flow cytometry. As shown in Figure 12, 93-95% of GFP^{+} CD11c^{int} cells were Ly49Q^{+}, indicating that GFP^{+} CD11c^{int} pDCs are largely a homogenous population consisting of mature pDCs.

In conclusion, pDCs can be identified in DPE^{GFP}xRAG-1$^{-/-}$ mice simply based on GFP expression. The implantation of these mice with B16-Flt-3L tumor cells results in marked expansion of pDC numbers within their natural environment *in vivo*.

6.2.3. Isolation of pDCs from Flt-3L-treated DPE^{GFP}xRAG-1$^{-/-}$ mice

Due to the requirement of several different markers for pDC identification, their purification has been difficult in the past. However, Flt-3L-treated DPE^{GFP}xRAG-1$^{-/-}$ mice facilitated isolation of pDCs simply based on GFP expression without any further manipulation (see Figure 13). Thus, pDCs were isolated by FACS from spleens of Flt-3L-treated DPE^{GFP}xRAG-1$^{-/-}$ with a routinely achieved purity of 95-98% (see Figure 13).

Figure 13: FACS-sorted GFP^{+} pDCs are highly pure.

Splenocytes from B16-Flt-3L implanted DPE^{GFP}xRAG-1$^{-/-}$ mice were sorted based on GFP expression. Numbers represent percentage of gated GFP^{+} pDCs of all cells prior to (left) and post sorting (right).

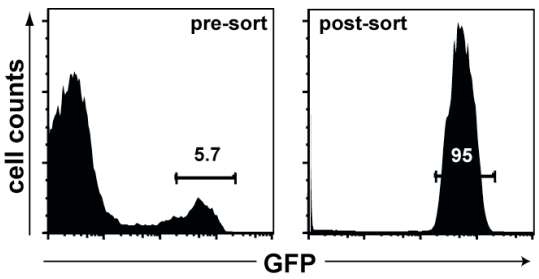

Purified pDCs were analyzed for their integrity and morphology. Cytospins of freshly isolated GFP^+ cells were stained with methylene blue and eosin and analyzed under a microscope. Consistent with previously published reports, GFP^+ cells revealed a round, plasma cell-like morphology (Figure 14A). Fluorescence microscopy of sorted cells confirmed that all of the cells exhibited a uniformly lymphocyte-like population that was green fluorescent (Figure 14B).

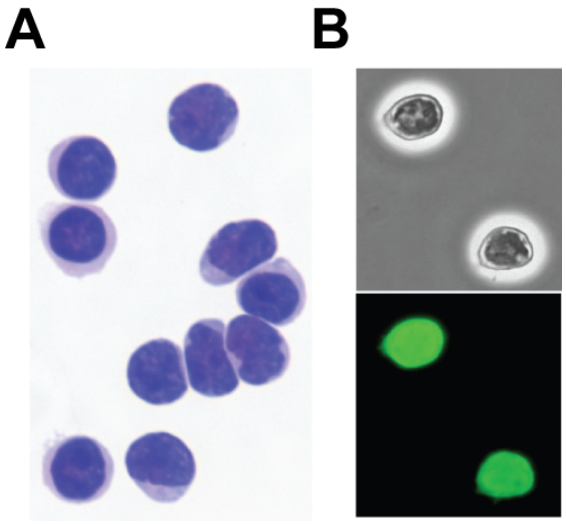

Figure 14: Sorted GFP^+ cells from splenocytes of a Flt-3L-treated $DPE^{GFP}xRAG\text{-}1^{-/-}$ mouse exhibit a plasma cell-like morphology.

(A) Cytospins of sorted pDCs were stained with methylene blue and eosin, and analyzed under a Nikon E600 upright microscope at a 40x magnification. **(B)** Sorted GFP^+ pDCs in suspension were imaged on a Nikon TE300 inverted microscope (magnification: 20x).

Collectively, our system allowed for a rapid isolation of high numbers of unmanipulated GFP^+ pDCs directly *ex vivo*.

6.2.4. pDCs stimulated with influenza virus A/PR/8 produce higher amounts of IFN-α than pDCs activated by CpG 1826, which express higher levels of costimulatory molecules

Since one of the hallmarks of pDCs is their production of type I interferons we tested the ability of GFP$^+$ cells to produce IFN-α. To this end, sorted GFP$^+$ cells were stimulated with either purified influenza virus A/PR/8 (PR8) or CpG 1826 oligonucleotide (ODN). As shown in Figure 15A, pDCs stimulated with PR8 virus released 10-fold higher levels of IFN-α as compared to pDCs stimulated with CpG 1826 (p=0.0076) (Figure 15A). pDCs cultured in medium alone did not produce IFN-α. In conclusion, pDCs activated by influenza virus were particularly privileged to secrete IFN-α when compared to CpG 1826-stimulated pDCs.

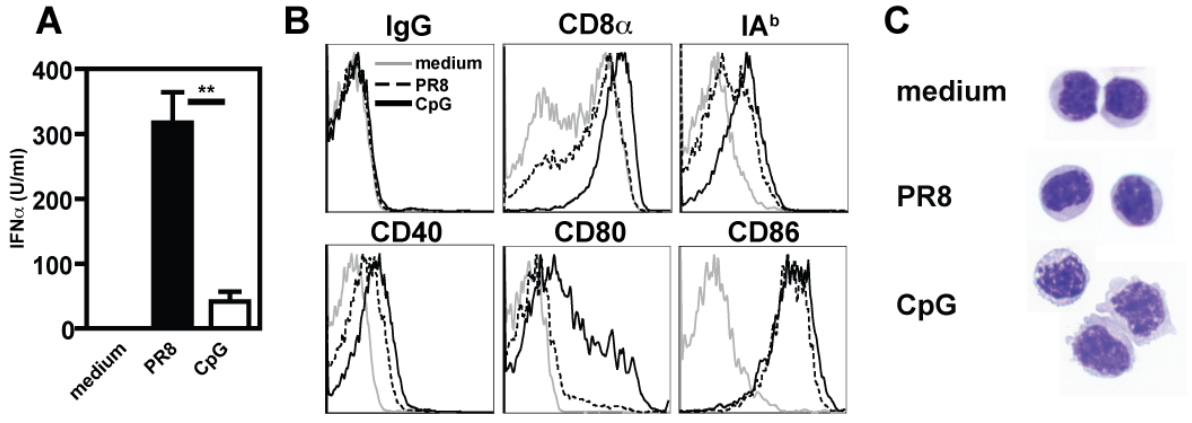

Figure 15: pDCs activated with influenza PR8 virus and CpG 1826 exhibit phenotypic and functional differences.

(A) Sorted GFP^{hi} pDCs were incubated for 24 h in medium, with 300 HAU/ml purified and UV-treated PR8 virus or 5 μg/ml CpG 1826 ODN. Supernatants were analyzed for IFN-α by ELISA. Results of two independent experiments are shown. **(B)** Sorted and treated GFP^{hi} pDCs (as in **A**) were stained for expression levels of IA^b, CD8α, CD40, CD80 and CD86 or a respective IgG control antibody and analyzed by flow cytometry. Representative results of one out of five independent experiments shown. (**C**) Cytospins of pDCs as in (**A**) reveal morphological differences between PR8- and CpG-stimulated pDCs.

pDCs and other DC subsets mature upon activation, a process that is accompanied by upregulation of costimulatory molecules such as CD40, CD80 and CD86. It had previously been shown that type I interferons are necessary for maturation of DC and pDCs following TLR-activation and viral infection [89, 128, 181, 182]. Thus, the hypothesis was addressed that pDCs activated by CpG may not have fully matured. pDCs were stimulated with either PR8 or CpG 1826 and the expression levels of costimulatory molecules were examined. As shown in Figure 15B, pDCs cultured in medium remained immature and expressed low levels of class II molecules and CD40, CD80 and CD86 (MFI (mean fluorescence intensity): 10, 4, 18, 16) in line with other publications [40]. Surprisingly however, these markers were highly upregulated in pDCs stimulated with CpG 1826 (MFI: IA^b 67; CD40 29; CD80 332). In contrast, PR8 induced the upregulation of costimulatory molecules to a markedly lower extent (MFI: IA^b 26; CD40 10; CD80 65) despite the high IFN-α-production. Interestingly, CD86 was similarly induced by either stimulus (CpG: MFI 627, PR8 577). Upregulation of CD8α was also observed, which was expressed in intermediate levels in unstimulated pDCs, but highly induced upon CpG-treatment and to a lower extend also on PR8-treated pDCs (MFI: untreated 162; PR8 228; CpG 564) [42]. Higher concentrations (up to 5000 HAU/ml) of virus and the use of live virus did not significantly increase the levels of costimulatory molecules (data not shown and [183]). When virus was added simultaneously with CpG 1826, pDCs upregulated costimulatory molecules to a level similar to CpG alone (data not shown) suggesting that CpG 1826 induced the maximum response in pDCs. In comparison with conventional $CD11c^{hi}$ dendritic cells, pDCs exhibited much lower surface expression of costimulatory molecules (data not shown).

CpG-activated pDCs also exhibited a differential morphology compared to pDCs activated by PR8 virus (Figure 15C). Cytospins of overnight-cultured pDCs stimulated with CpG 1826 showed a ruffled membrane and nuclei different in shape as compared to PR8 virus-activated pDCs. The round, plasmacytoid morphology of pDCs treated with PR8 virus was similar to pDCs cultured in medium alone.

In conclusion, there appeared to be a morphological, phenotypical and functional dichotomy of pDCs after stimulation with influenza virus PR8 and CpG 1826.

6.2.5. Maturation of PR8-activated pDCs but not CpG-activated pDCs is type I IFN-dependent

To assess whether the IFN-α production and upregulation of costimulatory molecules in PR8-activated pDCs may be dependent on a positive feedback loop of type I interferon signaling [128, 184], pDCs from Flt-3L-treated 129/Sv wild-type (WT) mice and mice that lack the IFNA receptor ($IFNAR^{-/-}$ mice) were sorted and cultured overnight under the conditions described above. IFN-α levels in supernatants of virus-stimulated pDCs from $IFNAR^{-/-}$ mice were significantly lower compared to IFN-α in the supernatant from WT mice ($p=0.006$). In contrast, the low induction of IFN-α by CpG 1826 in WT mice was not significantly influenced by the deficiency in IFNA-receptor expression (p=n.s.). These findings imply a crucial role for an autocrine type I interferon signaling loop to sustain high levels of type I IFN production by virus-stimulated pDCs. In contrast, CpG 1826-induced IFN-α production appeared to be independent of that feedback loop.

Consistent with the results obtained from GFP^{+} pDCs from $DPE^{GFP}xRAG\text{-}1^{-/-}$ mice, CpG 1826 induced higher levels of CD40 and MHC class II molecules in 129/Sv WT mice (Figure 16B). Interestingly, the upregulation of CD40 and CD86, but not MHC class II molecules, was significantly abrogated in virus-stimulated pDCs from $IFNAR^{-/-}$ mice. This difference may be due to different transcription factor binding sites in promoter elements of these molecules (such as NF-κB- and IRF-binding sites) [185]. In contrast, maturation of pDCs induced by CpG 1826 was independent of type I interferon feedback signaling. Collectively, these results (Figure 16A and B) suggested the involvement of different intracellular signaling pathways by PR8- and CpG-stimulated pDCs.

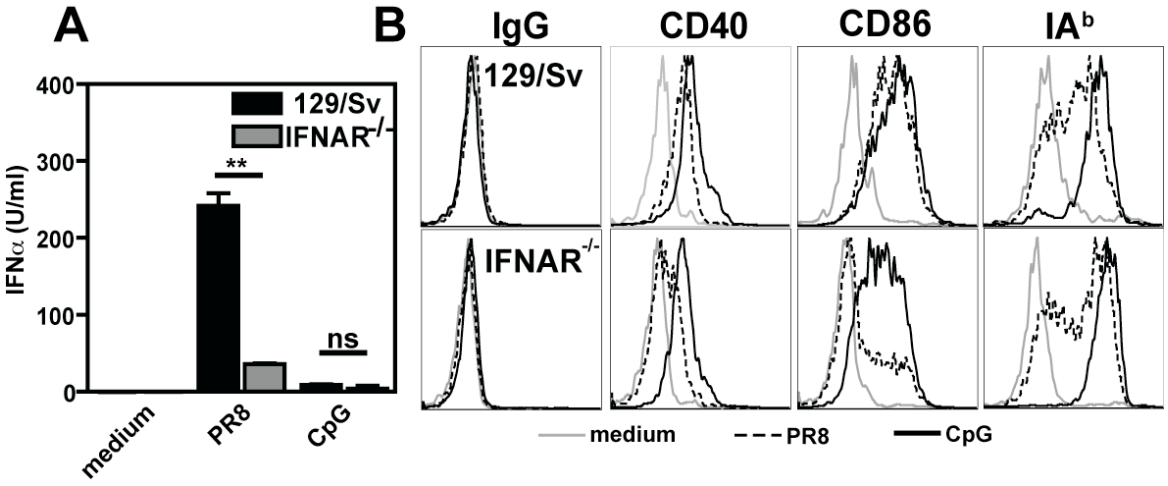

Figure 16: Type I interferon dependence of PR8-induced maturation in pDCs.

IFN-α production (**A**) and expression levels of costimulatory molecules (**B**) in pDCs sorted from spleens of Flt-3L-induced 129/Sv WT and IFNAR$^{-/-}$ mice. pDCs were cultured overnight in medium alone or with influenza virus PR8 virus or CpG 1826 (see Figure 15). Representative results of one out of two independent experiments are shown.

6.2.6. pDCs activated by CpG 1826 induce higher proliferation of T cells *in vitro* and *in vivo* compared to PR8-stimulated pDCs

Based on the observation that costimulatory molecules in pDCs stimulated by CpG 1826 and PR8 are differentially induced, we hypothesized that CpG-treated pDCs may exhibit an enhanced ability to present antigen to T cells. pDCs and conventional CD11c^{+} CD11b^{+} DCs were sorted and stimulated for 4 h with CpG 1826 or PR8 or, in case of DCs, with LPS. DCs were then pulsed with OVA peptide (SIINFEKL) (10 ng/ml) and added in increasing numbers to antigen-specific CD8^{+} T cells purified from OT-1 mice. After 72 h, [^{3}H]thymidine was added to cultures and radioactive incorporation was measured 16 hours later. As shown in Figure 17A, CpG-activated pDCs induced higher proliferation of T cells

than pDCs activated by influenza virus. However, $CD8^+$ T cells primed by pDCs proliferated poorly as compared to conventional DCs.

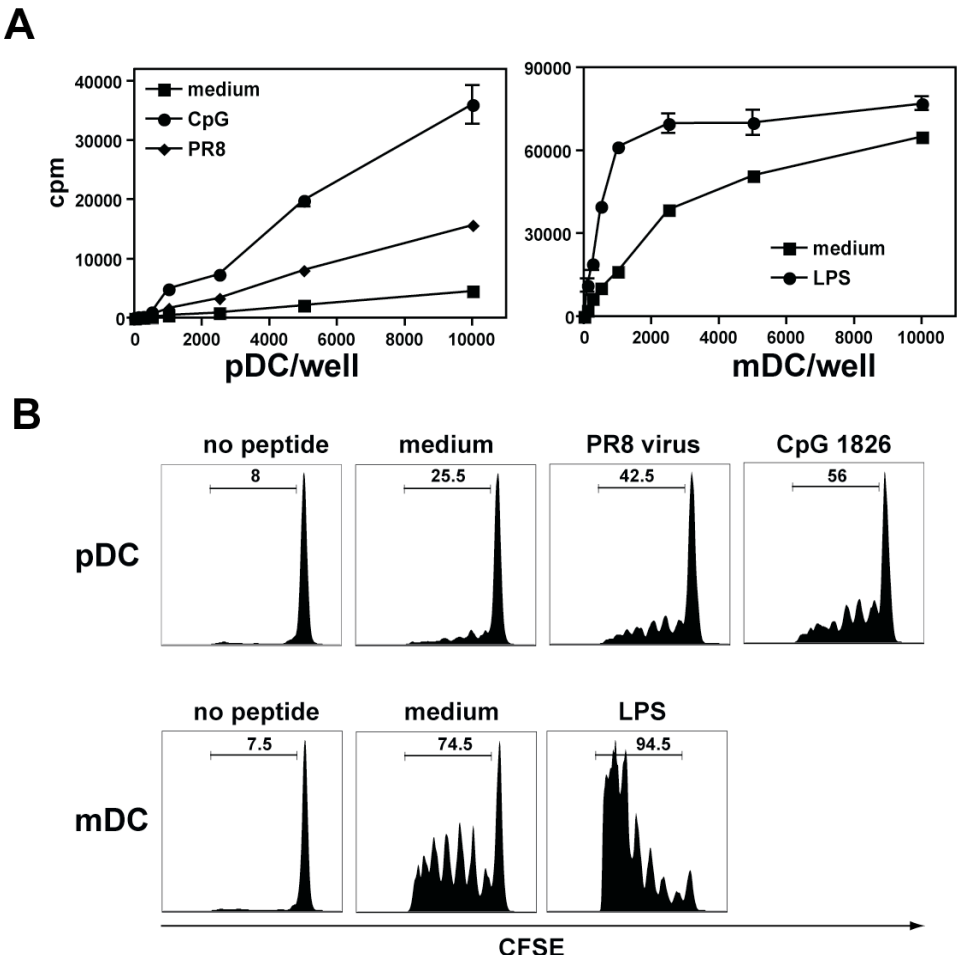

Figure 17: Stimulation with CpG 1826 confers peptide-pulsed pDCs a higher potential to induce proliferation of antigen-specific $CD8^+$ T cells than activation with PR8 virus

(A) Sorted DC populations were activated for 4 h as in Figure 15, and pulsed with 10 nM SIINFEKL-peptide in the final hour. DCs were cultured in increasing numbers with purified $CD8^+$ T cells from OT-1 mice for 72 hours. Co-cultures were pulsed with 1 μCi [^{3}H]thymidine for 16 hours before counting radioactive units. Representative results of one out of 3 independent experiments are shown. **(B)** $5x10^6$ CFSE-labeled $V\alpha2^+$ $CD8^+$ T cells from OT-1 mice were adoptively transferred into WT C57Bl/6 recipients at day -1. DC populations were prepared as in (**A**) on day 0 and $3\text{-}5x10^5$ cells injected i.v. into the recipients that had received T cells. Seventy two hours later, splenocytes were analyzed for CFSE dilution (gated on $V\alpha2^+$ $CD8^+$). Results of one out of 3 independent experiments are shown.

To confirm the results from the *in vitro* assays, DC subsets that were treated as described above were injected into WT mice that had received CFSE-labeled splenocytes from OT-1 mice. CFSE irreversibly couples to both intracellular and cell surface proteins by reacting with lysine side chains and other available amine groups. When cells divide, the CFSE label is distributed equally between the daughter cells, which are therefore half as fluorescent as the parents. As a result, decrease in cellular fluorescence intensity marks each successive generation of proliferating cells, which can be readily followed by flow cytometry. Spleens from recipient mice were harvested after 72 h and the CFSE profile of the transferred cells was analyzed. In homing assays (see chapter 2, Figure 28) it was established that adoptively transferred pDCs localize to spleen and to a lesser degree to PLNs. Thus, it was assumed that antigen-specific T cells would encounter pDCs preferentially in spleen. Consistent with the *in vitro* results, CpG-activated pDCs induced higher proliferation of T cells than virus-activated pDCs (Figure 17B, top row). MDCs, especially the LPS-treated mDCs (Figure 17B, bottom row), were much more potent in inducing $CD8^+$ T cell proliferation. Taken together, the data suggest that direct antigen presentation of pDCs may not be their main function.

6.2.7. Distinct transcriptome signatures define differentially activated pDCs

6.2.7.1. Change in gene transcripts of pDCs activated by PR8 virus and CpG 1826

While the above described experiments pointed towards the possibility that pDCs may differentiate into two discrete populations in response to PR8 virus and CpG 1826, the analyses thus far were limited to comparing a select panel of phenotypic and functional readouts. To further gain insight into changes in pDCs induced by both stimuli, we assessed

their global transcriptional profile with Microarray chips. One of the major advantages of this method is that it allows for simultaneous observation of the expression of thousands of genes and their coordinate change in a given condition. To this end, RNA was isolated from sorted pDCs after culture for 1 h and 4 h with CpG 1826, PR8 virus or medium alone. Samples were generated in 2-3 independent experiments, and hybridized to the Affymetrix MOE430v2.0 chip. The total number of probes on this chip is 45,000, which represent 39,000 transcripts and variants from over 34,000 murine genes. Differentially expressed genes were identified based on their p-values with a cut-off determined by a 3-way ANOVA with a 5% FDR using the Partek Software. Subsequently, an additional fold difference ≥2.0 on the replicates resulted in the number of changed probes in the pairwise comparisons that are summarized in the following table (see Table XI).

Condition	Number of significantly changed genes
medium 1 h - 4 h	210
medium 1 h - PR8 4 h	2377
medium 1 h - CpG 4 h	5371
medium 4 h - PR8 4 h	1532
medium 4 h - CpG 4 h	4565
CpG 4 h - PR8 4 h	1318
PR8 1 h - PR8 4 h	2189
CpG 1 h - CpG 4 h	5390

Table XI. Numbers of significantly changed probes in pairwise comparisons of the microarray data from differentially activated pDCs.

(see information in the text)

A high number of genes was identified that changed under any given culture condition. Different probes pDCs cultured in medium alone for 1 h and for 4 h. 2377 different probes were observed when pDCs were stimulated with PR8 virus (PR8) for 4 h compared to medium 1 h. The highest number of changes were observed when pDCs were cultured with CpG 1826 for 4 h (5371). The numbers in the comparisons medium 1 h - CpG 4 h (5371) and CpG 1 h - CpG 4 h (5390) as well as medium 1 h – PR8 4 h (2377) and PR8 1 h – PR8 4 h (2189) were very similar. This was due to the fact that stimulation for 1 h with either CpG or

PR8 virus resulted only in minor changes in gene transcript expression levels. Therefore, the focus of the microarray analysis was directed mostly to the changes observed after 4 h of stimulation.

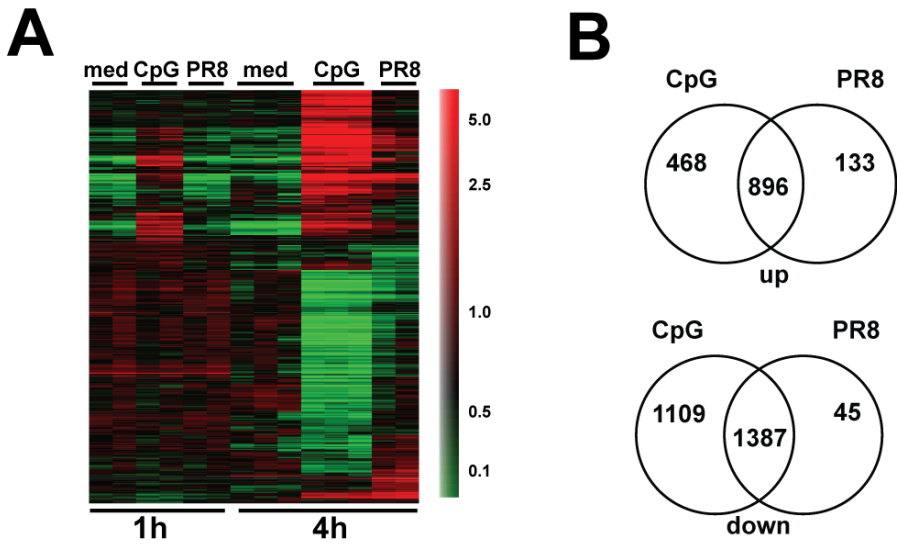

Figure 18: Identification of differentially induced genes in pDCs activated by PR8 virus and CpG 1826

(A) Gene tree of 462 statistically significant different genes between CpG 1826- and PR8 virus treated pDCs calculated based on a 3-way ANOVA. Color bar represents median of the expression level of each gene across all 14 samples (red color depicts up-, green color represents downregulation). **(B)** Venn Diagrams of up- and downregulated genes that are specific for either CpG- or PR8 virus treatment or shared by both. Genes from gene lists medium 1 h - CpG 4 h and medium 1 h - PR8 4 h (with significant genes based on p-values from the ANOVA) that changed >2-fold under the respective other condition were subtracted. Remaining genes with a >3-fold induction over medium 1 h value were graphed.

In a first overview it was determined how many genes were significantly different between pDCs treated with PR8 compared to pDCs activated with CpG 1826. In a statistical analysis with pairwise comparisons using the Partek software (excluding different times), 462 genes were calculated to be significantly different. In a gene tree compiled by using the GeneSpring software, genes clustered as depicted in Figure 18A with a higher expression of

175 genes in CpG- and 287 genes in PR8-stimulated cells, respectively. The replicates of different experiments appeared very similar to each other as shown by close color matches. Only a minor number of genes were differentially regulated after 1 h of stimulation comparing both conditions. This set of genes represented mostly genes categorized as "response to biotic stimulus" (EASE-score 2.73e-11, NIH-DAVID) and were upregulated exclusively by CpG at 1 h. While most changes in gene expression were observed at 4 h but not 1 h after stimulation, the number of 462 genes represents an underestimation of different genes between CPG and PR8-activated pDCs, because only those genes were found to be significant in the time-independent comparison, if they had changed in the same direction and to a similar degree in both the 1 h and the 4 h comparisons.

Thus, in a different analysis approach using gene expression in medium 1 h as the baseline, the stimulus-specific changes after 4 h of culture were calculated based on the gene lists from the pairwise comparisons (see Table XI, CpG: 5371 and PR8: 2377, respectively). As displayed in a Venn Diagram, we identified 896 and 1387 genes that were up- or downregulated, respectively under both conditions (Figure 19B). However, a select panel of genes was uniquely regulated by either stimulus, i.e. for CpG 468 up- and 1109 downregulated genes; and for PR8 virus 133 up- and 45 downregulated genes (Figure 18B).

6.2.7.2. Differential induction of IFN-α genes and transcripts of costimulatory molecules by PR8 virus- and CpG 1826- activated pDCs

In agreement with the above results obtained by ELISA (Figure 15A), the microarray data revealed specific upregulation of several genes of the IFN-α family in pDCs stimulated by PR8 virus, which was up to 100-fold lower in CpG 1826-treated pDCs (Figure 19A). Interestingly, changes in IFNb gene expression were very similar between both stimuli, which suggests that certain promoter sequences of type I IFN genes may be differentially regulated. Indeed, the IFNa4 promoter displays different requirements for members of the

IRF family and does not contain NF-κB-binding sites, whereas the IFNb promoter does [186].

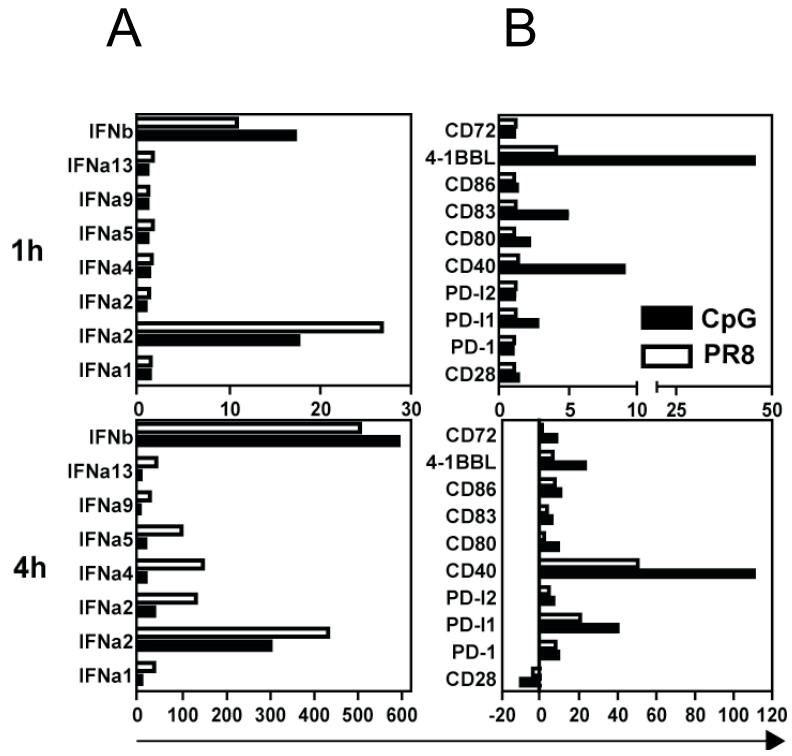

Figure 19: Induction of genes from the IFN-α and IFN-β family and upregulation of costimulatory molecules in pDCs stimulated with PR8 virus and CpG 1826.

Mean fold change of expression values of IFNa and IFNb genes (**A**) and costimulatory molecules (**B**) in pDCs after 1 h (top graphs) or after 4 h (bottom graphs) of stimulation with CpG 1826 ODN (black bars) and PR8 virus (white bars). Gene expression of pDCs cultured in medium for 1 h was taken as baseline.

When analyzing costimulatory molecules, an early robust upregulation of transcripts for 4-1BBL, CD40 and CD83 was observed specifically in CpG 1826-stimulated pDCs (Figure 19B). Neither the expression of PD1 nor PD-L2, negative immune regulators, was significantly changed at either time point. However, PD-L1 was upregulated 40-fold and 20-fold by CpG 1826 and PR8, respectively. CD28 was downregulated after 4 h under both conditions. Induction of the TRAIL, TNFSF10, was specific for PR8-activated pDCs (17-fold

and 5-fold with PR8 and CpG, respectively (see supplemental Table for PR8-specific genes, Table XIX). TRAIL may mediate cytotoxic activity of virally activated pDCs [95]. In addition, Sema6D, a new member of the semaphorin family, which are believed to play a role in costimulatory activity [187], was found to be exclusively induced by CpG 1826 (100-fold vs. 7-fold in PR8-activated pDCs) (see supplemental Table for CpG-specific genes, Table XXI).

Collectively, the microarray data of IFN-α genes and transcripts of costimulatory molecules mirror the distinct type I interferon production and the phenotypic profile described at the protein level after 24 h (see above, chapter 6.2.4.).

6.2.7.3. Differential cytokine and chemokine expression profiles by pDCs activated by PR8 virus and CpG 1826

In addition to IFN-α, pDCs can produce other soluble mediators such as chemokines and cytokines. Until now, cytokines analyzed after activation of pDCs have mostly been limited to type I interferon and IL-12. Therefore, we aimed to fully characterize the level and kinetics of expression of soluble mediators in pDCs stimulated with CpG 1826 and PR8 virus.

Within 1 h of stimulation, elevated transcription of CXCL2, CCL3 and CCL4 in CpG 1826-treated, but not virus-activated pDCs was observed, which increased further after 4 h (see Figure 20A). In addition, CpG 1826 also induced transcription of CCL5 as well as XCL1 and CXCL9, CXCL10 and CXCL11. Interestingly, whereas the transcriptional level of CCL2 in virus-activated pDCs did not change during that time, they had increased RNA-levels of CCL3, CCL4 and CCL5 after 4 h, albeit significantly lower as compared to CpG-stimulated pDC. These results indicate a kinetic difference for the induction of these chemokines by both stimuli. Moreover, these data corroborate recent findings by Banchereau's group analyzing the kinetic chemokine response of human blood pDCs in response to influenza virus. They showed that pDCs have a temporally regulated program to secrete different chemokines [120]. At 4 h of stimulation, the transcriptional level of XCL1 and the three

known CXCR3 ligands (CXCL9, CXCL10 and CXCL11) were induced to a similar extent in PR8-activated pDCs (MIG: CpG 56 vs. PR8 175; IP-10: CpG 234 vs. PR8 301; I-TAC: CpG 18 vs. PR8 53; fold induction over medium 1 h), and suggests a possible role of these chemokines in attracting cells during viral infection to sites of infection such as the lung.

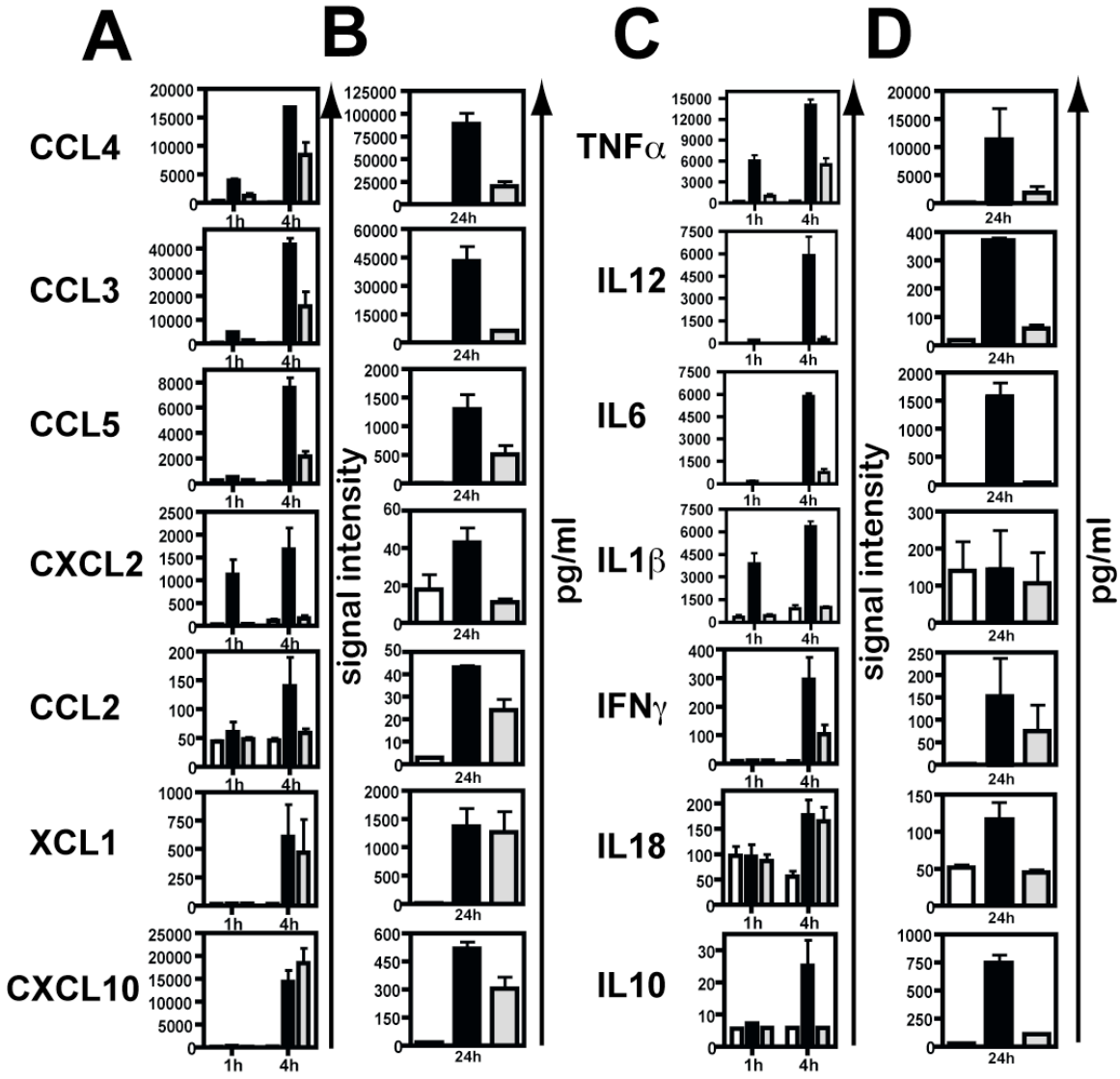

Figure 20: Cytokine and chemokine production of pDCs in response to CpG and PR8 virus activation.

(A and B) Chemokine and **(C and D)** cytokine expression levels (A and C: microarray analysis (1 h and 4 h), B and D: Multianalyte profiling of supernatants of cultured pDCs (24

h)). White bars: pDCs in medium, dark bars: CpG 1826-treated pDCs, grey bars: PR8 virus-treated pDCs. Results of 2 independent experiments shown as mean ± SEM. Of note: Analysis of IL12b for microarray and IL12p70 in supernatants.

In addition, it was observed that the panel of cytokines produced by CpG 1826-activated pDCs contrasted those induced by influenza virus. Gene transcripts for TNF-α, IL-6 and IL-12 were expressed very highly with CpG, but much less with PR8 (Figure 20C). Interestingly, CPG 1826 also induced negative mediators in pDCs, such as Ebi3, which is part of the cytokine IL-27, that is important in negatively regulating Th17 cells. Another cytokine with negative immunoregulatory function, IL-10, which may counteract the high level of pro-inflammatory cytokines such as IL-12 [188], was induced by CpG 1826 as well.

Next, the chemokine and cytokine mRNA expression profiles were verified at the protein level. To this end, the supernatants of CpG 1826 and PR8 stimulated pDCs were subjected to multianalyte profiling. As shown in Figure 20B and D, the secretion of the tested mediators correlated well with the mRNA levels. An exception was IL-1β, which was highly expressed at the mRNA level, but was not detected in the supernatants.

We further assessed the production of IL-12, TNF-α and IFN-γ by intracellular cytokines staining (ICS) on pDCs isolated *ex vivo* from a site of inflammation. For this purpose, DPE^{GFP} mice were injected intraperitoneally with Thioglycollate and cells that accumulated in the peritoneal cavity were harvested. As will be discussed in chapter 2, pDC numbers increase in the peritoneal cavity over 72 h in this model, where they remained immature in the absence of TLR ligands (see Figure 30). Peritoneal exudate cells were collected and cultured either in medium alone or in the presence of PR8 virus or CpG 1826. pDCs cultured in medium were negative for the cytokines tested, and only a low percentage of IL-12^+ (3%) and TNF-α^+ (10%) cells were detected after PR8 activation (Figure 21B). In contrast, 30% and 64% of GFP^{hi} $B220^+$ pDCs stained positive for IL-12 and TNF-α (Figure 21B), respectively, correlating well with the microarray results and amounts of these cytokines in the supernatant after *in vitro* stimulation. IFN-γ was undetectable in *ex vivo* activated pDCs. Indeed, IFN-γ-

production by murine pDCs has been shown to require IL-4 [189], suggesting special activation condition beyond the TLR ligands used in this study for its expression.

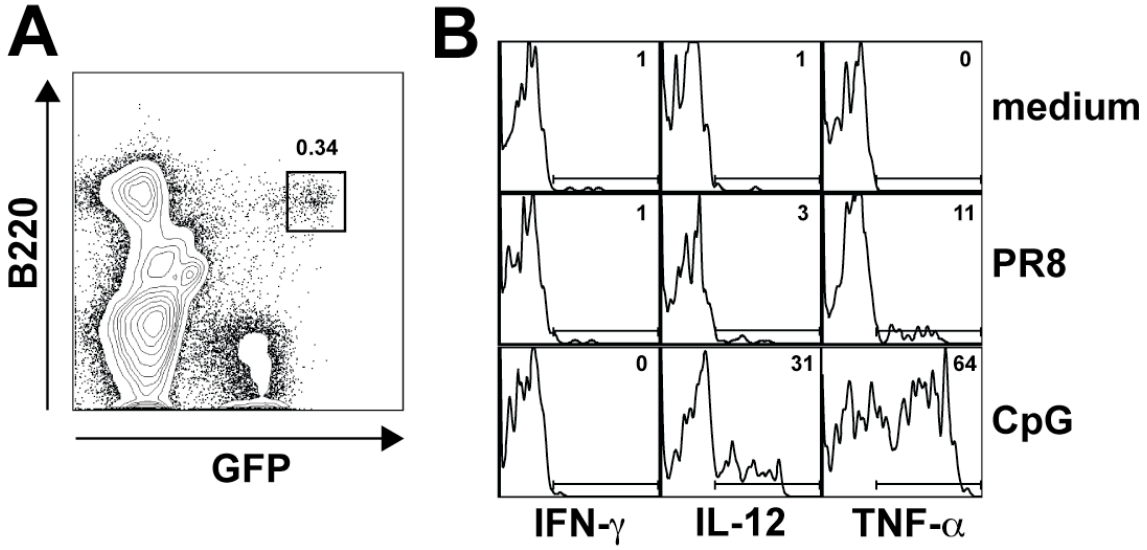

Figure 21: Cytokine production of pDCs *ex vivo* in a peritonitis model.

(A) DPE^{GFP} mice were injected i.p. with 1 ml of 3% (w/v) Thioglycollate and PECs were harvested after 68 h. Numbers represent percentage of GFP^{hi} $B220^{+}$ cells of total cells. (**B**) PECs were incubated for 4 h in presence of Brefeldin A in medium, with 375 HAU/ml purified and UV-inactivated PR8 virus or 5 μg/ml CpG 1826. pDCs were identified by staining with αB220. Intracellular cytokine staining was performed and results for IFN-γ, IL-12 and TNF-α are shown (gated on GFP^{hi} $B220^{+}$ pDCs). One representative experiment out of two is shown.

Taken together, the results presented here indicate that pDCs stimulated under the two conditions specialize with respect to the cytokines they secrete; pDCs activated by virus produce a select panel of chemokines as well as high levels of type I IFNs, while CpG 1826-stimulated pDCs release a broad panel of pro- and also anti-inflammatory mediators.

6.2.7.4. Induction of distinct signaling pathways by pDCs activated by PR8 virus and CpG 1826

It is conceivable that the distinct phenotypic and functional characteristics resulted from a difference in intracellular cell signaling pathways downstream of the TLRs. Indeed, a unique panel of differentially induced transcription factors was identified. IRF7 and STAT1 necessary for type I interferon production, were found to be expressed significantly higher following viral stimulation (Figure 22). Following CpG treatment, the expression of class II transactivator, C2ta, was higher as compared to PR8-activated pDCs. This is in line with higher levels of class II molecule expression by CpG 1826-activated pDCs (see Figure 15). Cited2, a CREB-binding protein/p300-interacting protein, was highly induced by CpG-stimulation including other transcription factors such as c-Myc, c-Rel and Iκ-Bζ, also known as Mail. It has recently been shown that CpG-activated pDCs from NF-κB1$^{-/-}$c-Rel$^{-/-}$ mice mounted a normal type I interferon response, however they were inefficient in IL-6 and IL-12 production [79]. Mail was upregulated 30-fold by CpG within 1 h of stimulation whereas PR8 induced its transcription only about 3-fold. Yamamoto et al. could demonstrate that Mail-deficient macrophages have impaired IL-6 production in response to TLR ligands [190]. Together with the results presented here this may indicate an important role for this transcription factor in production of inflammatory cytokines specific for CpG also in pDCs.

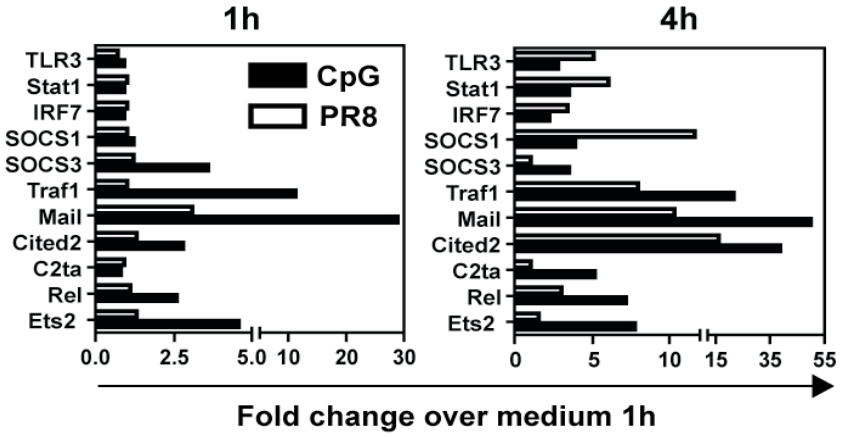

Figure 22: Fold induction of genes involved in Toll-like receptor signaling pathways and transcription of cytokines.

Mean fold change of expression values indicated genes in pDCs after 1 h (left) or after 4 h (right) of stimulation with CpG 1826 (black bars) and PR8 virus (white bars).

As factors involved in signaling can be regulated not only at the transcriptional level but also through posttranslational modifications, the results described above led us to the hypothesis that intracellular signaling represented by kinase-activation/-phosphorylation may be regulated differentially in pDCs activated by CpG 1826 or PR8 virus. Especially interesting was the group of stress-activated kinases, such as extracellular signal-related kinases (ERK) 1 and ERK2, p38 mitogen-activated protein kinase (MAPK) and their function in NF-κB-activation for induction of inflammatory cytokines. In human pDCs, it has been shown that p38 MAPK is also involved in IFN-α induction following TLR9 activation by CpG [75, 78], however the involvement of p38 upon TLR7 engagement has not been studied. Thus, pDCs were sorted and stimulated for 15 min. (15'), 45' and 3 h. Cell lysates were then subjected to analysis of ERK1/2-activation and Iκ-B-degradation. In unstimulated, freshly sorted pDCs, p-ERK1/2 levels were undetectable (Figure 23A). In contrast, ERK1 (p44) and to a lower extent ERK2 (p42) were transiently phosphorylated (peak at 45') following CpG 1826 activation (Figure 23A). Interestingly, phosphorylation of ERK1 showed different kinetics in PR8-stimulated pDCs, with a peak at 3 h. On the other hand, the time course of Iκ-B-degradation was similar in response to both stimuli.

For the analysis of p38-phosphorylation, we employed a flow cytometry-based assay. After the indicated times of culture, cells were fixed in 1.6% PFA, treated with methanol for permeabilization [170], stained for phospho-p38 and subsequently analyzed. With CpG 1826 but not PR8 virus, increased levels of phospho-p38 were observed within 45' of stimulation and remained elevated throughout the time points 3-5 h after activation (Figure 23B and C).

From these results and the differences in the microarray data it was concluded that pDCs mount a distinctly regulated intracellular signaling response to CpG 1826 and influenza PR8 virus with a diverse kinetic pattern. As a result, a high number of transcription factors, in

particular those involved in induction of pro-inflammatory responses, are highly induced by CpG but not PR8.

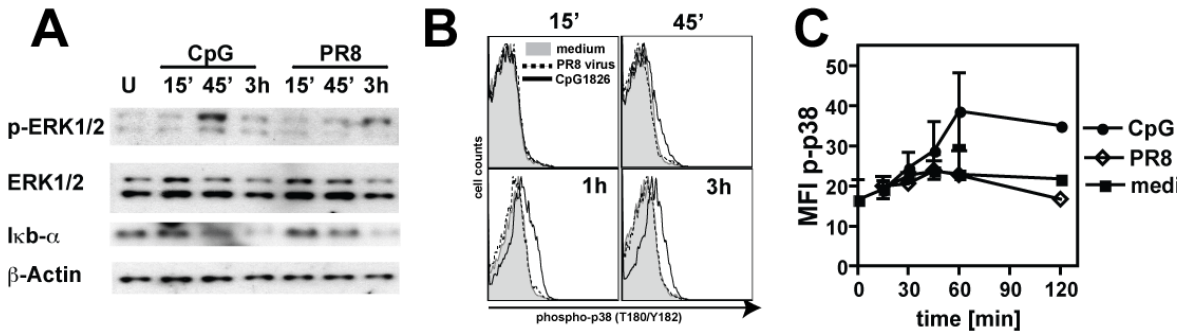

Figure 23: CpG 1826 induces p38- and ERK1-phosphorylation in pDCs.

(**A**) pDCs were sorted from spleens of Flt-3L-treated $DPE^{GFP}xRAG\text{-}1^{-/-}$ mice and left untreated (U) or stimulated with CpG 1826 or PR8 virus for the indicated times. Cell lysates were analyzed by immunoblot to detect ERK1/2 and Iκ-B. Blot of one representative out of 3 independent experiments is shown. (**B**) Total splenocytes from Flt-3L-treated $DPE^{GFP}xRAG\text{-}1^{-/-}$ mice were incubated in medium (grey histogram), with influenza PR8 virus (dashed line), or CpG 1826 (solid line) for the indicated times. Fixed and permeabilized cells were stained with antibodies against CD45R/B220 and p-p38 and analyzed by flow cytometry. Gates were set on GFP^+ $B220^+$ cells. Results of representative flow cytometry profiles out of 4 independent experiments are shown. (**C**) Mean fluorescence intensity (MFI) of p-p38 staining from cultured pDCs (as in **B**) was graphed over time.

6.2.7.5. Comparable upregulation of antiviral and interferon-stimulated genes in pDCs activated by PR8 virus or CpG 1826

Besides their production of type I interferons after encounter of the virus, other antiviral factors produced by pDCs have not been studied in detail. Thus, we investigated whether such genes may be induced by PR8 virus and CpG 1826 ODN in pDCs.

Among the best described genes and their products are interferon-stimulated genes (ISG), such as members of the IFIT family, proteins with tetratricopeptide motifs, which

inhibit protein synthesis, ISG15, an ubiquitin-like protein that conjugates numerous proteins and probably direct their degradation, and ISG20 3' to 5' exonuclease with specificity for ss-RNA [191]. The microarray results showed a major increase of the RNA transcripts of those genes in the range of 20-200fold (compared to their RNA-levels in pDCs in medium) in activated pDCs independent of the stimulus used (Table XII). Similarly, Mx proteins, a family of GTPases, which block binding of viral components and their intracellular transport, were upregulated 10- and 40-fold (Mx1 and Mx2), respectively.

Symbol	Common gene name	Genebank accesion	CpG vs medium 4h	PR8 vs medium 4h	PR8/CpG
RIG-1	retinoic acid inducible protein 1	BG063981	**7.2**	**16.3**	**2.2**
Prkr	protein kinase, interferon-inducible double stranded RNA dependent	BE911144	**12.5**	**18.9**	**1.5**
Mx1	myxovirus (influenza virus) resistance 1	M21039	**41.9**	**40.5**	**1.0**
Mx2	myxovirus (influenza virus) resistance 2	BC007127	**9.8**	**12.9**	**1.3**
Ifit1	interferon-induced protein with tetratricopeptide repeats 1	NM_008331	**219.6**	**274.8**	**1.3**
Ifit2	interferon-induced protein with tetratricopeptide repeats 2	NM_008332	**51.1**	**82.1**	**1.6**
Ifit3	interferon-induced protein with tetratricopeptide repeats 3	NM_010501	**45.3**	**113.7**	**2.5**
Igtp	interferon gamma induced GTPase	NM_018738	**13.0**	**13.2**	**1.0**
Tgtp	T-cell specific GTPase	NM_011579	**14.5**	**18.6**	**1.3**
AW111922	interferon G inducible GTPase	BM239828	**19.5**	**27.5**	**1.4**
Ifi1	interferon inducible protein 1	NM_008326	**5.0**	**6.9**	**1.4**
Ifi16	interferon inducible protein 16	NM_008329	**26.8**	**24.3**	**0.9**
Ifi30	interferon gamma inducible protein 30	NM_023065	**-1.9**	**-1.6**	**0.8**
Ifi35	interferon inducible protein 35	AW986054	**5.5**	**5.7**	**1.0**
Ifi47	interferon gamma inducible protein 47	NM_008330	**3.5**	**3.7**	**1.0**
Isg20	interferon-stimulated protein	BC022751	**95.1**	**120.5**	**1.3**
G1p2	interferon, alpha-inducible protein, isg 15	AK019325	**33.3**	**36.0**	**1.1**
USP18	ubiquitin specific peptidase 18	NM_011909	**21.9**	**22.4**	**1.0**
Ifi203	interferon activated gene 203	AI607873	**7.8**	**9.2**	**1.2**
Ifi205	interferon activated gene 205	AI481797	**6.6**	**6.7**	**1.0**
Oas1g	2'-5' oligoadenylate synthetase 1G	BC018470	**19.3**	**20.7**	**1.1**
Oas1b	2'-5' oligoadenylate synthetase 1B	BC012877	**1.8**	**2.5**	**1.4**
Oas2	2'-5' oligoadenylate synthetase 2	AB067535	**5.3**	**6.1**	**1.1**
Oas3	2'-5' oligoadenylate synthetase 3	AB067534	**54.6**	**53.1**	**1.0**
Oasl1	2'-5' oligoadenylate synthetase-like 1	AB067533	**19.4**	**20.5**	**1.1**
Oasl2	2'-5' oligoadenylate synthetase-like 2	BQ033138	**15.2**	**18.9**	**1.2**
Pml	promyelocytic leukemia protein, tripartite moti-containing protein 19	NM_008884	**3.8**	**6.2**	**1.6**
mda5	helicard	AY075132	**41.9**	**42.0**	**1.0**
RNAseL	ribonuclease L (2', 5'-oligoisoadenylate synthetase-dependent)	BF714880	**-1.5**	**1.7**	**2.0**
2510004L01Rik	viperin	BB132493	**71.8**	**72.5**	**1.0**
Serpini1	neuroserpin	NM_009250	**12.4**	**7.5**	**1.7**

Table XII. Upregulation of viral-induced and interferon-stimulated genes in pDCs stimulated with influenza PR8 virus and CpG 1826.

Fold induction of genes induced by CpG and PR8 stimulation was calculated as the ratio of replicate intensities at 4 h to the average intensity of medium control at 4 h. PR8/CpG represents the ratio of fold values from PR8 to CpG-stimulated pDCs.

Moreover, transcripts for PKR (protein kinase dsRNA regulated), which causes translation inhibition by phosphorylation of the translation initiation factor eIF2, and the helicase RIG-I were up to 20-fold increased. Oligoadenylate synthetases activate endoribonucleases responsible for degradation of viral RNA. Several members were expressed in pDCs and highly induced after activation (2-50-fold). Stimulation of pDCs also led to an increase of IFI16 and other members of the P200 protein family shown to impair cell proliferation and inhibition of rRNA transcription. We identified viperin (cig5), a potential antiviral effector protein [192], to be 70-fold upregulated in activated pDCs.

In conclusion, independent of the stimulus used in our system, we observed strong induction of the transcription of several antiviral genes in activated pDCs that may contribute to their role in immune responses.

6.2.8. pDCs acquire discrete phenotypes during influenza virus infection or after injection with CpG 1826 *in vivo*

Having established that pDCs can differentiate into two phenotypically and functionally distinct subsets *in vitro*, it remained to be shown that they acquire similar phenotypes also *in vivo*. To this end, DPE^{GFP} mice were infected by intranasal administration of live PR8 influenza virus. The expression of costimulatory molecules on pDCs isolated from the lung-draining mediastinal lymph node, spleen and lungs were analyzed in a time course. Within 3 days post infection, a major percentage of pDCs (gated on GFP^{hi} $B220^{+}$ cells) expressed CD86 in the infected lung (Figure 24A, top row, solid line). At the peak of the immune response, around day 7-8 post infection, virtually all pDCs in the lung were $CD86^{+}$. In

contrast, pDCs in lungs maintained low levels of CD40 expression throughout the infection (Figure 24A, top row, dotted line). pDCs in the medLN and spleen exhibited a $CD40^{low}$ $CD86^{low}$ phenotype (Figure 24A, bottom row and data not shown).

To investigate the effects of CpG 1826 *in vivo*, DPE^{GFP} mice were injected intravenously with CpG mixed with DOTAP, a liposomal reagent [18, 128]. The phenotype of activated pDCs was analyzed in spleen 20 h later. As shown in Figure 24B, pDCs from mice injected with CpG upregulated not only CD86, but also CD40, CD80 and class II molecules, thus differing from pDCs activated during PR8 virus infection.

Taken together, the data of pDCs activated *in vivo* corroborated the observed phenotypes of pDCs after PR8 and CpG 1826 stimulation *in vitro*.

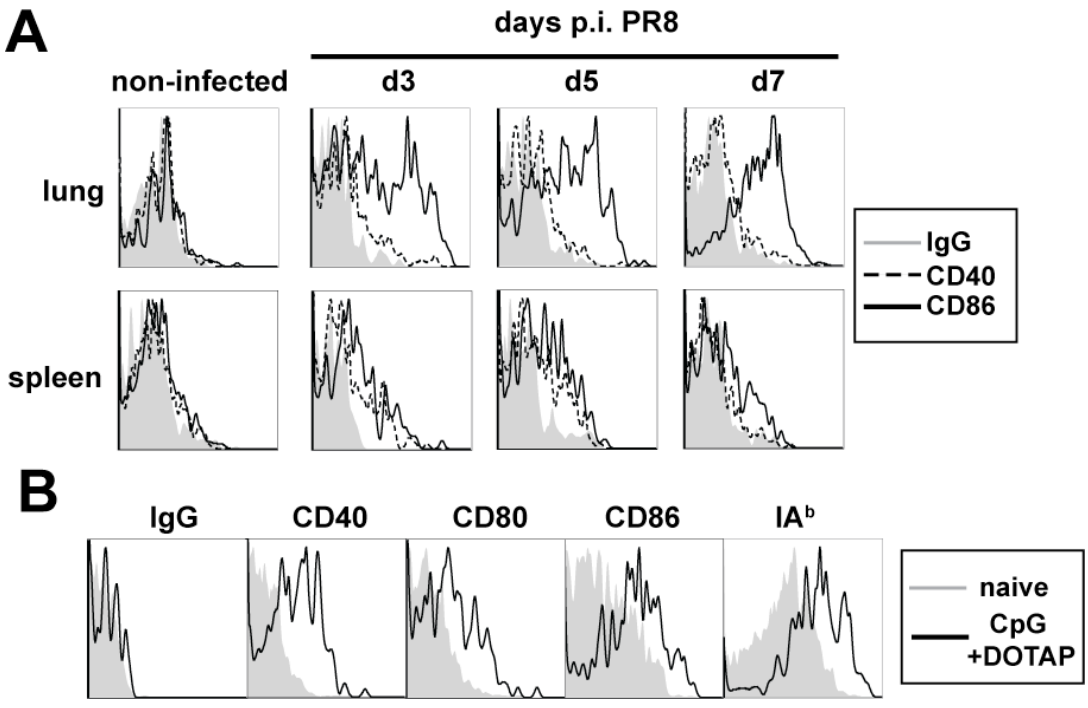

Figure 24: Phenotype of GFP^{hi} pDCs *in vivo* following PR8 virus infection and injection with CpG 1826.

(A) DPE^{GFP} mice were infected intranasally with 500 $TCID_{50}$ in 50 μl of PBS. At 3, 5 and 7 days post infection, lungs and spleens were processed and stained for CD45R/B220, and costimulatory molecules. Histograms depict expression of CD40, CD86 and staining with an isotype control antibody (gated on GFP^{hi} $B220^{+}$ pDCs). One representative out of 3 independent experiments is shown. **(B)** DPE^{GFP} mice were injected i.v. with 20 μg CpG 1826 mixed with 15 μl DOTAP in 200 μl PBS. 20h later, GFP^{hi} $B220^{+}$ pDCs in the spleen were analyzed for the expression level of costimulatory molecules. One out of 2 independent experiments is shown.

6.3. Discussion

Toll-like receptors are known to play a crucial role in the innate recognition of ubiquitous pathogens through conserved motifs. It has been previously demonstrated that pDCs express TLR7 and TLR9, which recognize microbial components, including ss-RNA of influenza virus, and CpG-containing DNA, respectively. Upon activation, pDCs undergo a differentiation process that has been characterized by the production different levels of pro-inflammatory mediators. This has led to the concept that pDCs are capable of responding to various stimuli with a high degree of flexibility. Moreover, pDCs have been shown to perform a wide range of actions in various diseases. Thus, certain functions of pDCs are harmful and have been implicated in autoimmune diseases or cancer, whereas others are beneficial in the defense against microbes. We addressed the question of how pDCs can exert this broad spectrum of actions by characterizing in-depth their response to prototypic TLR ligands at the cellular and molecular level.

We demonstrated that PR8 virus- and CpG 1826-activated pDCs differ in their maturation states, including expression of costimulatory molecules, and cytokine and chemokine profiles both on the transcriptional and on the protein levels. Our findings support a model proposing that pDCs can be polarized into two distinct populations: type I interferon-producing pDCs generated by activation with PR8 virus, and CpG-stimulated pDCs with higher levels of costimulatory molecules and increased production of pro-inflammatory cytokines. It is likely that both subsets may have distinct roles during different immune response settings.

For our studies we made use of a recently described transgenic mouse strain, DPE^{GFP}, in which pDCs express high levels of GFP [178, 179]. When crossed to mice deficient in lymphocytes, pDCs remained the only GFP^{hi} cells in the spleens of these animals. Subcutaneous implantation of tumor cells modified to express Flt-3 ligand increased total numbers of splenic pDCs *in vivo*. Thus, this system provides a major advantage over the use

of bone marrow-derived, *in vitro*-cultured pDCs, as they are maintained in their natural environment *in vivo*. Furthermore, GFP-expression enables us to isolate pDCs without manipulation and exposure to antibodies, which potentially alters their function.

In agreement with previous findings, it was confirmed that GFP^{hi} pDCs from DPExRAG-$1^{-/-}$ mice reveal a plasma cell-like lymphoid appearance (Figure 14A and B). Although the GFP^{hi} cells represent a uniform population based on morphologic criteria, it is possible that these cells may harbor subsets that respond differently to certain stimuli. It has been proposed that two pDC subpopulations exist, a $CD4^+$ and a $CD4^-$ subset [175, 193]. $CD4^-$ pDCs may represent the immediate precursor of the $CD4^+$ subset. We found that the splenic GFP^{hi} pDC population contained $CD4^+$ (~95%) and $CD4^-$ (~5%) cells. In addition, two pDC populations have been distinguished in the bone marrow, but not in the peripheral lymphoid organs based on the expression of Ly49Q (~50% $Ly49Q^+$) [55, 56]. In our hands, splenic GFP^{hi} pDCs were largely $L49Q^+$ (93%) (Figure 12). Thus, the paucity of $CD4^-$ and $Ly49Q^-$ subsets within the GFP^{hi} pDC population could not account for the observed differences after PR8 and CpG 1826 stimulation. Using RAG-1/GFP reporter gene mice, another study proposed the existence of subpopulations with different functional properties in the bone marrow, termed pDC1 and pDC2 [57]. It is unknown whether these subsets are also amplified in the spleens of Flt-3L treated animals, and whether they respond differently to CpG 1826 and PR8 virus stimulation. While we cannot formally exclude that GFP^{hi} pDC contain pDC1 and pDC2 subsets, our phenotypic data show that these cells respond relatively uniformly to stimulation. Thus, the entire population upregulated CD86 and MHC class II expression to the same extent (Figure 15). In contrast, pDC1 and pDC2 differentially regulate these genes after CpG exposure [57]. We therefore conclude that it is unlikely that the GFP^{hi} pDC population harbors those subsets with different receptiveness to the utilized stimuli.

Stimulating pDCs with the prototypic TLR7 agonist ss-RNA influenza virus and the TLR9 ligand unmethylated CpG 1826 ODN resulted in a large number of phenotypic and functional differences. GFP^{hi} pDCs activated by PR8 virus produced high levels of IFN-α (Figure 15A). In contrast, CpG 1826 induced only marginal secretion of IFN-α in pDCs.

However, the expression of the costimulatory molecules CD40, CD80 and MHC class II was much higher in CpG 1826-treated pDCs (Figure 15B). Furthermore, we found that the maturation of pDCs isolated from IFNAR$^{-/-}$ mice was impaired following activation with influenza virus but not with CpG 1826, suggesting that the autocrine feedback loop of type I interferons is imperative for sustaining differentiation of PR8-virus-activated pDCs (Figure 16B) [89, 128, 181, 182]. These data are consistent with previous findings that CpG class-B ODN induces only weak IFN-α-responses in pDCs, and that the response is triggered in an IFNAR-independent pathway (Figure 16A) [177].

Although many previous studies have reported that pDCs can differentiate into cells with antigen presenting capabilities and induce T cell proliferation [96, 103, 104, 175, 194], the involvement of pDCs in naïve T cell priming remains controversial. Conflicting results may be explained by the difficulties in obtaining pure pDCs *ex vivo*. In contrast to other findings [101, 104], PR8-activated pDCs in our hands had a markedly low impact on CD8$^+$ T cell proliferation (Figure 17). On the other hand, pDCs activated by CpG 1826 exhibited a greater capacity of stimulating antigen-specific CD8$^+$ T cells, and it is likely that the higher levels of costimulatory molecules expressed on CpG-activated pDCs account for this observation. It is possible that PR8 virus- and CpG 1826-activated pDCs may display different survival properties, which may contribute to their differential effect on T cell proliferation *in vivo*. Previous experiments have demonstrated that pDCs localize to T cell areas of the spleen after adoptive transfer and should therefore have access to naïve T cells (data not shown). In these experiments, the numbers of pDCs remained relatively constant for at least 72-96 h, which should be sufficient for the cells to make contact with T cells. Taken together, these data suggest that pDCs are poor inducers of T cell proliferation in comparison to conventional mDCs, suggesting that antigen presentation by pDCs may not be their main function.

By employing microarray chip analysis, we have identified a large number of uniquely regulated genes in pDCs induced by PR8 virus and CpG 1826 (Figure 18). Similar to a previous study in mDCs [195], these results suggest that different stimuli can induce distinct programs in pDCs that may result in optimized functions against a given pathogen.

Furthermore, tt has previously been shown in pDCs that CpG type A ODN, which are strong inducers of IFN-α, localize to a distinct endosomal compartment and have different retention times as compared to CpG type B ODN, which induce only low amounts of IFN-α [177, 196-199]. Although both CpGs are ligands for TLR9, the nature of the ligand may dictate the functional response. It is therefore conceivable that the response to CpG type A ODN may resemble that of PR8 virus. It is also possible that other surface receptors may contribute as co-receptors in the initiation of distinct responses, as has been recently suggested [70].

In accordance with other data, we defined differential regulation of positive and negative intracellular TLR signaling components, which may explain the different responses of pDCs activated by CpG 1826 and PR8 virus (Figure 22). Common to both TLR7 and TLR9 is the recruitment of the adaptor molecule MyD88 and TRAF6 in a complex together with members of the IRAK family, which results in the phosphorylation of IRF7, IRF5 and STAT1/2-activation. This pathway is essential for type I interferon induction [71-75]. On the other hand, signals transmitted through stress-activated kinases of the MAPK-, ERK- and JNK-family lead to Iκ-B degradation and the activation of the transcription factor NF-κB. It has previously been shown that NF-κB is essential for the production of pro-inflammatory cytokines and chemokines, as well as IFN-α induction in pDCs [75, 78]. Interestingly, we could demonstrate that the RNA-level of the transcription factors c-Myc, c-Rel and Mail are specifically increased upon CpG-activation in pDCs and may contribute to the induction of inflammatory cytokines. While we found that degradation of Iκ-B followed a similar time course in pDCs after stimulation with PR8 virus and CpG 1826 (Figure 23A), we observed distinct differences in the kinetics of ERK1/2 phosphorylation in pDCs. Moreover, p38 MAPK was consistently phosphorylated only after CpG 1826 stimulation of the cells (Figure 23B and C). This is in line with earlier observations that CpG rapidly induces p38 and ERK-phosphorylation in myeloid cells, such as DC and monocytes and macrophages [78, 200, 201]. Of note, however, when we used a p38-inhibitor (SB202190), we found decreased upregulation of costimulatory molecules in both CpG 1826 and PR8-activated pDCs cultured overnight (data not shown). However, the interpretation of these inhibition studies is difficult,

as autocrine IFN-signaling through the type I IFN-receptor can also activate signaling pathways involving p38-MAPK.

Despite the described differences, we also identified an overlap of similarly induced transcripts in pDCs after CpG 1826 and PR8 stimulation, exemplified by interferon-stimulated and antiviral stress-induced genes. These results imply that activated pDCs must share a partly common program to upregulate genes with antiviral functions (Table XII). The presence of a core response pattern for pDCs regardless of the stimulus may be beneficial for an anti-pathogenic response. Similar results have been observed by a study that analyzed the different profile of dendritic cells in response to the pathogens Escherichia coli, Candida albicans and influenza virus [195].

While we have learned a great deal about the functions of pDCs from *in vitro* studies, their functional characterization during diseases *in vivo* remains important in order to understand their contribution to immune defense and pathology. *In vivo* studies have been hampered by the fact that markers specific for pDCs under steady-state conditions are also expressed on other immune cells during inflammation. Therefore, the unequivocal identification of pDCs during infection, or in autoimmunity, has been challenging. The fact that CpG- and virus-matured pDCs remained GFP^{hi} in our model enabled us to identify these cells during influenza infection and after CpG 1826 application *in vivo*. Consistent with our *in vitro* results, pDCs in the lungs of infected mice expressed high levels of CD86, but not CD40 and CD80. In contrast, CpG 1828 induced high levels of costimulatory molecules and class II on pDCs. These results indicate that pDCs can adapt the phenotypes described after *in vitro* stimulation also *in vivo*. As a consequence, we can ask what could be the functional significance of two distinct differentiation states of pDCs *in vivo*? After viral activation, pDCs appear to be poised to produce antiviral mediators, including type I IFNs (Figure 15 and Figure 19). In addition, they secrete chemokines CXCL9, CXCL10 and XCL1 (Figure 20), which may be involved in attracting T cells and NK cells to the lung during influenza virus infection [120, 123]. The fact that these cells show an incomplete induction of costimulatory molecules suggests that they may not be directly involved in T cell priming.

PDCs may have tolerizing functions, induce T cell anergy and/or the generation of regulatory T cells. Thus, it will be important to determine whether the only partial induction of these molecules is causally involved in these phenomena. Moreover, in certain viral and autoimmune diseases it has been shown that IFN-α, in contrast to IL-12 and TNF-α, may be detrimental for recovery [188, 202]. After injection of CpG 1826, pDCs differentiated into cells with a more mature phenotype (with respect to expression of costimulatory molecules), and released higher levels and a broader panel of pro-inflammatory cytokines and chemokines (Figure 15, Figure 20, Figure 24). These data are of clinical relevance, as ongoing human trials are examining the efficacy of various CpG ODN as adjuvants to enhance immune responses [203, 204].

In summary, we deciphered in detail the differences of pDCs activated by two different TLR7 and TLR9 ligands, PR8 virus and CpG 1826 ODN. Based on our results we propose that murine pDCs can be polarized into separate populations. Despite an overlapping panel of antiviral genes, the distinct expression profiles of pro-inflammatory mediators and costimulatory molecules indicate the capability of pDCs to adopt distinct differentiation states following their activation. We expect that further elucidation of the molecular mechanisms of their generation and the investigation of their precise roles during infection, autoimmunity and cancer will contribute to our understanding of the pathogenesis of disease.